BULLETIN OF THE POLISH ACADEMY OF SCIENCES
TECHNICAL SCIENCES, Vol. 71(6), 2023, Article number: e146796
DOI: 10.24425/bpasts.2023.146796

Controlling bifurcations in high-speed rotors utilizing active gas foil bearings

Anastasios PAPADOPOULOS, Ioannis GAVALAS, and Athanasios CHASALEVRIS*

National Technical University of Athens, Athens, Greece

Abstract. High-speed rotors on gas foil bearings (GFBs) are applications of increasing interest due to their potential to increase the power-to-weight ratio in machines and also formulate oil-free design solutions. The gas lubrication principles render lower (compared to oil) power loss and increase the threshold speed of instability in rotating systems. However, self-excited oscillations may still occur at circumferential speeds similar to those in oil-lubricated journal bearings. These oscillations are usually triggered through Hopf bifurcation of a fixed-point equilibrium (balanced rotor) or secondary Hopf bifurcation of periodic limit cycles (unbalanced rotor). In this work, an active gas foil bearing (AGFB) is presented as a novel configuration including several piezoelectric actuators that shape the foil through feedback control. A finite element model for the thin foil mounted in some piezoelectric actuators (PZTs), is developed. Second, the gas-structure interaction is modelled through the Reynolds equation for compressible flow. A simple physical model of a rotating system consisting of a rigid rotor and two identical gas foil bearings is then defined, and the dynamic system is composed with its unique source of nonlinearity to be the impedance forces from the gas to the rotor and the foil. The third milestone includes a linear feedback control scheme to stabilize (pole placement) the dynamic system, linearized around a speed-dependent equilibrium (balanced rotor). Further to that, linear feedback control is applied in the dynamic system utilizing polynomial feedback functions in order to overcome the problem of instability.

Key words: bifurcation control; Hopf bifurcation; active gas foil bearings; high-speed rotors; nonlinear control.

1. INTRODUCTION

In their conventional design, gas foil bearings are self-acting machine elements designed to support high-speed rotating machines. They utilize an oil-free technology by creating a thin load-carrying gas film, without the need for external pressurization, see [1]. Furthermore, because of the absence of contact between the rotor and the internal shell of the bearing, it was found that low power loss could be achieved, as described by H. Heshmat *et al*. in [2]. Over the past few decades, there has been a rapid development of GFBs and their applications, especially in small turbomachines. Moreover, there is an ever-increasing interest in the application of GFBs in turbocharging systems, and small jet engines for UAVs.

GFBs at their conventional design include a deformable top and bump foil. Specific materials are used in real applications to accommodate friction in boundary lubrication regimes during the journal lift-off at relatively low speeds. The effective damping of a conventional gas foil bearing is sourced in gas flow properties, the friction between the top foil and the bump foil, and the friction between the bump foil and the outer rigid shell. In general, the deformable top foil benefits the energy dissipation mechanism and the load capacity of the bearing, simultaneously. Low or minor damping portion is sourced on the internal damping (material damping) of the coupled components, which are steel alloys in most applications. The energy dissipation mechanism is therefore quite complex, and in theoretical prediction, it strongly depends on the respective model applied for the deformation and the dynamics of the components. As expected, the bump foil stiffness and damping (sourced in Coulomb friction), together with the effective damping from the gas flow, influence significantly the threshold speed of instability of the rotating shaft (journal) [3]. Similarly to oil-lubricated bearings, gas foil bearings suffer from negative effective damping and self-excited oscillations at speeds higher than the threshold speed of instability, which restricts the operating range of the rotor-bearing system as high amplitude oscillations appear.

The need for controllable GFBs arises from the requirement to improve the dynamic characteristics of the supported high-speed (or ultra-high-speed) rotors, such as the suppression of the oscillation amplitudes and the elimination of instabilities within a wide range of rotating speeds. Different computational models for GFBs are presented in [3–8] along with the numerical and experimental results concerning the response of the considered rotors. Also, investigation of the stability margins of rotating systems supported by GFBs is implemented in [9–11].

The necessity for adaptability to different operational conditions, such as ambient temperature or unbalance conditions led to significant research in this direction, and a significant effort was made for the design and development of controllable or active GFBs (AGFBs). The most frequently used method is the placement of piezoelectric actuators in the circumferential direction of the bearing, between the top foil and the rigid shell. J. Park and K. Sim proposed an active gas foil bearing (AGFB) with a laminated top foil, a classic bump foil, and piezo

*e-mail: chasalevris@mail.ntua.gr

Manuscript submitted 2023-05-07, revised 2023-07-14, initially accepted for publication 2023-07-18, published in December 2023.

stacks aiming to accommodate the clearance by adjusting the thickness of the piezo stacks and mechanically preloading the bearing by modifying the elongation of those piezo stacks, as described in [12]. It was found that the clearance control had a positive impact on the dynamic force coefficients of the system, whereas the preload control had a slighter one. On the other hand, a large preload results in a safer passage through the critical speeds. Additionally, L. Savin *et al*. explain in detail the most common controllable bearing system, as described in [13]. Recent works on the adaptability of journal bearings in operating conditions can be found, among several others, in [14–16]. Regarding active GFBs, radial air injection was introduced by S. von Osmanski and I.F. Santos in [17]. In any case, the goal was the safe passage through critical speeds, the increase of the damping force coefficients, and the suppression of the amplitudes of the oscillations for medium unbalance grades.

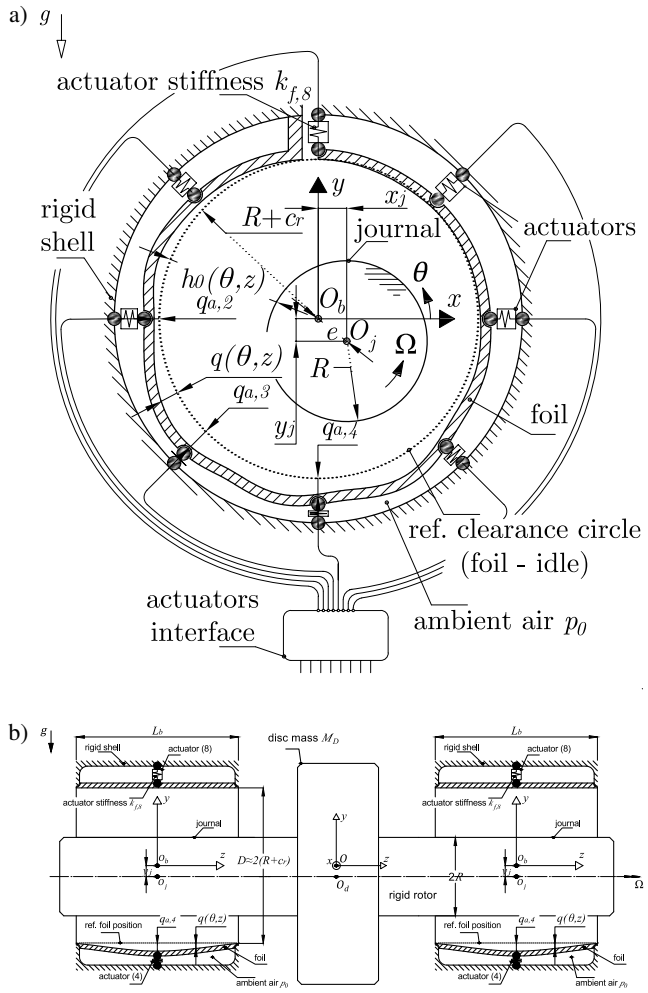

Fig. 1. Representation of a) the active gas foil bearing suggested in this work and b) the rigid shaft carrying a disc located at its center, mounted on two AGFBs

In this work, another concept of active gas foil bearing is introduced. The AGFB consists of a rigid shell (bearing sleeve), a thin top foil and piezoelectric actuators allowed to move radially, see Fig. 1a. The bump foil is neglected and the actuators are connected directly to the top foil. The performance of the AGFB is tested in a simple rotating system, composed of two identical AGFBs and a rigid rotor with a disc located in its center, as shown in Fig. 1b. No misalignment is considered. The top foil is modelled using the finite element method (FEM) and the resulting matrices are reduced using the static (Guyan) reduction method, described in [18]. The Reynolds equation governing the compressible gas lubrication is discretized with the finite difference method (FDM). The differential state equations concerning the rotor motion are then derived by Newton's law. Simulation results are presented for two bearing diameters, D30 and D100, for different layouts of actuator placement and different values of the disc mass. A linear control method using an observer is used in order to stabilize unstable fixed points of the balanced system. Also, a linear polynomial feedback control law is used in order to eliminate secondary Hopf bifurcations of the balanced system, as proposed by Yu and Chen in [19]. The same feedback law is used to suppress the oscillation amplitudes and produce synchronous output signals.

2. PHYSICAL AND ANALYTICAL MODEL OF THE ROTOR-AGFB SYSTEM

2.1. Computational model for the deformable foil

The foil of the AGFB, see Fig. 1a, is assumed to behave as a thin flat plate and the state equations are derived using the MZC (Melosh–Zienkiewicz–Cheung) finite element, described in [20]. The piezoelectric actuators are added to mount the foil. A high stiffness value is assigned to all actuators. After the construction of the FE mesh, each node is allowed to be displaced perpendicular to the mid-surface of the plate. Those deflections are considered as the radial displacements of the foil. Also, each node is allowed to perform two rotations around the two axes that are perpendicular to the normal vector of the plate surface. These rotations are not included in the reduced model as the static (Guyan) condensation is applied. The finite element mesh along with the placement of the actuators for the two bearings is shown in Figs. 2a and 2b.

As shown, twelve actuators are used for the bearing D30 and twenty-four for the bearing D100. The actuators in the middle plane are always moving according to the desired control feedback law, while the actuators in the front and rear planes can be either moving or static. In both cases, sixteen elements are considered in the circumferential direction and ten in the axial. Both bearings have a length-to-diameter ratio $L_f/D = 1$. An indicative foil deformation $\Omega = 700$ rad/s is exhibited in Fig. 2c.

In this theoretical study, strong idealizations apply regarding the modelling of the actuators and their mounting in the rigid shell and the top foil. In reality, the contact surface of the actuator and the moving foil or the outer rigid shell will not be discrete as assumed in this work. Further to that, the modelling of actuator stiffness and damping follows in an approximation of the values for the characterization of piezoelectric actuators presented in [21–23] and the control loop for the positioning of actuators is not included in the current model. Further to that, the foil deformation may experience a slightly different magnitude when different finite elements are utilized. The foil defor-

mation in general is a challenging problem, especially for small bearings like D30 or lower, due to the high curvature. Considering the above, the theoretically predicted benefit of stabilization, presented in below, is most likely overestimated.

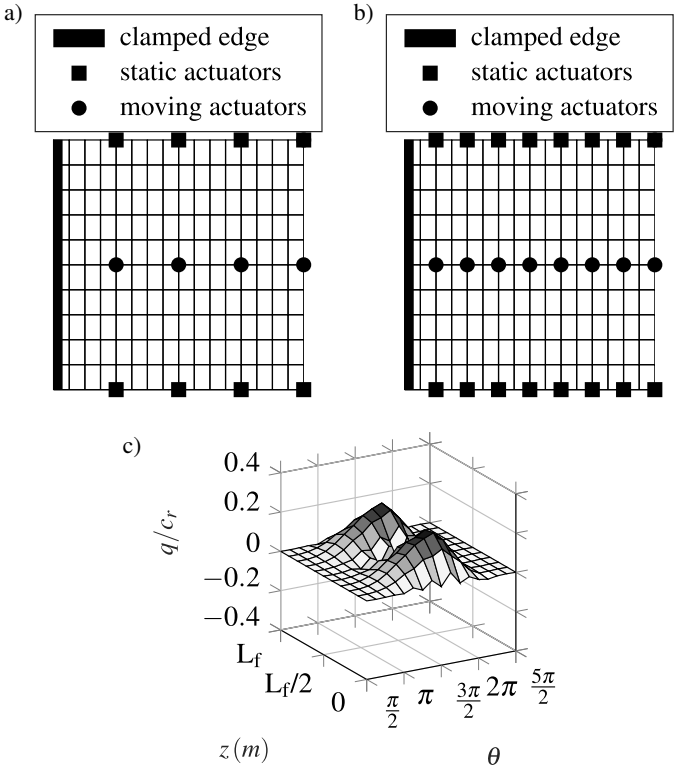

Fig. 2. Finite element mesh and placement of the actuators for the AGFB of a) D30, and b) D100. c) typical foil deformation at $\Omega =$ 700 rad/s for D100, and $m_d = 1$ kg

The resulting state equations of the foil are shown in equation (1), where $\mathbf{F}_r$ is the reduced vector containing the gas forces, $\mathbf{F}_{\text{act}}$ is the vector containing the actuator forces and $\mathbf{q}$ is the vector containing the radial displacements of the nodes of the finite element mesh. The actuator forces are calculated as $F_{\text{act}_{ij}} = k_{f_j}\left(q_{a_j} - q_i\right)$, where k_{f_j}, and q_{a_j} are the stiffness and the elongation of the j-th actuator, respectively. Also $\mathbf{M}_r$, $\mathbf{C}_r$, $\mathbf{K}_r$ is the reduced mass, damping, and stiffness matrix of the foil structure, respectively, where $\dot{q}$ is the derivative concerning time t:

$$\begin{Bmatrix}\dot{\mathbf{q}}\\ \ddot{\mathbf{q}}\end{Bmatrix} = \begin{bmatrix}\mathbf{0} & \mathbf{I}\\ -\mathbf{M}_r^{-1}\mathbf{K}_r & -\mathbf{M}_r^{-1}\mathbf{C}_r\end{bmatrix}\begin{Bmatrix}\mathbf{q}\\ \dot{\mathbf{q}}\end{Bmatrix} + \begin{Bmatrix}\mathbf{0}\\ \mathbf{M}_r^{-1}\left(\mathbf{F}_r + \mathbf{F}_{\text{act}}\right)\end{Bmatrix}. \tag{1}$$

2.2. Solution of the elasto-aerodynamic lubrication problem

The Reynolds equation governing the phenomenon of compressible fluid lubrication is derived, taking into account the following assumptions: the gas film is isothermal, the flow is laminar, the fluid inertia is negligible, the fluid is ideal, i.e. $p/\rho_{\text{air}} = ct$, where ρ_{air} is the density of the lubrication mean (air), there are no fluid leaks, $R_f = R + c_r \approx R$, where R is the radius of the rotor and c_r is the bearing clearance and the pressure does not change in the radial direction, see [24]. Under those assumptions, the Reynolds equation is transformed into a system of ODEs, by using a central FD approach only for the spatial partial derivatives, see equation (2). The computational mesh for the application of the FD method is the same as the mesh used for the FEM. The Reynolds equation is:

$$\dot{p} = \frac{h^2}{12\mu}\left(p_x^2 + p_z^2\right) + \frac{ph}{4\mu}\left(h_x p_x + h_z p_z\right) + \frac{ph^2}{12\mu}\left(p_{xx} + p_{zz}\right) - \frac{R\Omega}{2}p_x - \frac{R\Omega p}{2h}h_x - \frac{p}{h}\dot{h}, \tag{2}$$

where $h(t,\theta,z) = c_r - x_j(t)\cos(\theta) - y_j(t)\sin(\theta) + q(t,\theta,z)$ is the thickness of the gas film and x_j, y_j are the lateral displacements of the centre of the disc in x and y directions respectively. In equation (2), p_χ is the partial derivative of the pressure p with respect to χ (circumferential direction) and p_z is the partial derivative of the pressure p with respect to z (axial direction). For the solution of equation (2), boundary and initial conditions are required. Dirichlet boundary conditions are applied to each boundary of the domain, setting the pressure to be equal to the ambient one. Also, at a time $t = 0$, the pressure is considered to be equal to the ambient one for every node of the domain (initial conditions). The boundary conditions and the initial conditions are defined in equation (3).

$$\begin{gathered} p(t,0,z) = p(t,2\pi,z) = p_0 \rightarrow p_{1,j}(t) = p_{N_X+1,j}(t) = p_0\,,\\ p(t,\theta,0) = p(t,\theta,L_f) = p_0 \rightarrow p_{i,1}(t) = p_{i,N_Z+1}(t) = p_0\,,\\ p(0,\theta,z) = p_0\,. \end{gathered} \tag{3}$$

The resulting gas forces, see Fig. 3a, acting on the rotor are calculated as:

$$\begin{aligned} F_{B,X} &= -\sum_{i=2}^{N_X}\sum_{j=2}^{N_Z}\left(p_{i,j} - p_0\right)\cos\left(\theta_i\right)\Delta\chi\Delta z,\\ F_{B,Y} &= -\sum_{i=2}^{N_X}\sum_{j=2}^{N_Z}\left(p_{i,j} - p_0\right)\sin\left(\theta_i\right)\Delta\chi\Delta z, \end{aligned} \tag{4}$$

where N_X and N_Z are the number of intervals in the circumferential and axial direction of the computational domain, respectively, and the corresponding pressure distribution is shown in Fig. 3b. Note that if the value of the pressure at a node of the computational domain falls below the ambient value, then, at that node, the pressure will be considered equal to the ambient. The validity of the numerical solution applying finite difference method has been recently verified in [25] comparing to the existing literature for applications in conventional GFBs including bump foil structure.

2.3. Rigid rotor on AGFBs and composition of the full nonlinear system

The forces acting on the rotor are of three types: gas forces, see equation (4), gravity forces, and unbalance forces. Unbalance forces are centrifugal forces appearing on the rotor due to the

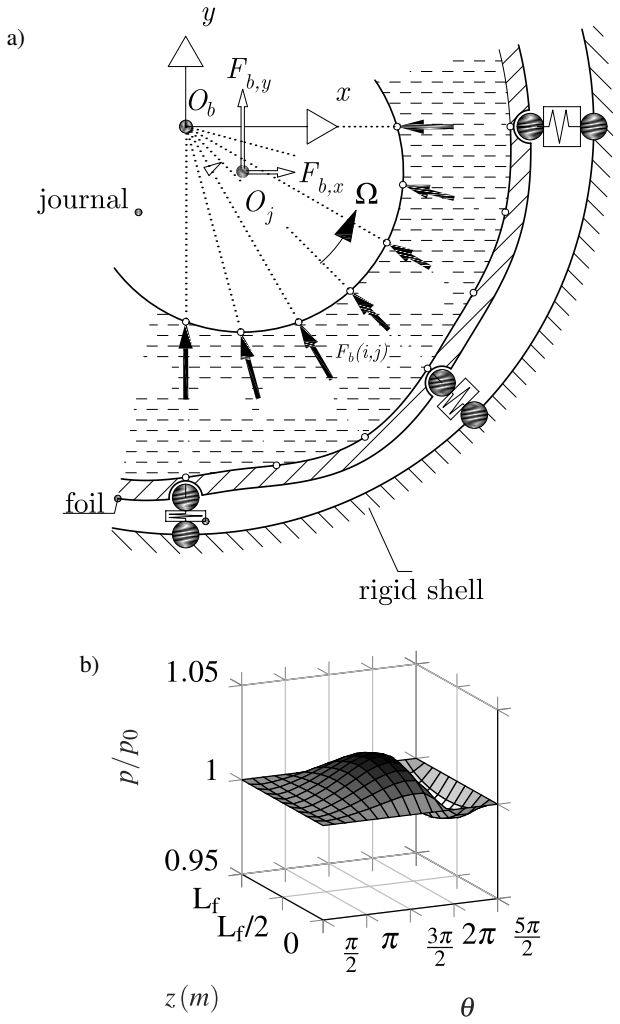

Fig. 3. a) representation of the gas forces acting on the rotor and the foil, and b) typical pressure distribution at $\Omega = 700$ rad/s for D100, and $m_d = 1$ kg

non-uniformly distributed mass of the disc and the rotational speed. This leads to vibrations that often need to be suppressed. The unbalance force in the x-direction is denoted by F_{U_X} and in the y-direction by F_{U_Y}. For constant rotational speed, these unbalance forces are:

$$F_{U,X} = m_d e_u \Omega^2 \cos(\varphi_r), \quad F_{U,Y} = m_d e_u \Omega^2 \sin(\varphi_r), \tag{5}$$

where $\varphi_r = \Omega t$ and m_d is the mass of the disc.

The unbalance eccentricity e_u is calculated according to the ISO unbalance G-grades. In this work medium (G2.5) and high (G6.3) unbalance grades will be considered. The disc unbalance is of magnitude $u = m_d e_u$ and the eccentricity is $e_u[m] = 0.001G/\Omega_r$, where Ω_r denoting the maximum service speed in rad/s. The state equations of the rotor are

$$\begin{aligned} \dot{x}_1 &= x_2, \quad \dot{x}_2 = \frac{F_{B,X}}{m_d} + \frac{F_{U,X}}{m_d}, \\ \dot{x}_3 &= x_4, \quad \dot{x}_4 = \frac{F_{B,Y}}{m_d} + \frac{F_{U,Y}}{m_d} - g, \end{aligned} \tag{6}$$

where $x_1 = x_j$, $x_2 = \dot{x}_j$, $x_3 = y_j$, $x_4 = \dot{y}_j$.

It is important to note that the two journal centers and the disc centre execute identical planar motions as the rotor is rigid and no tilting motion is considered in the rotor kinematics. Therefore, only the journal kinematics is considered in the state feedback control (see Section 3). Taking into account the state equations of the foil, equation (1), of thepressure field, equation (2), and of the rotor, equation (6), the full system is written in the form:

$$\dot{\mathbf{x}} = \mathbf{f}(t, \mathbf{p}, \mathbf{q}, \dot{\mathbf{q}}, \mathbf{x}_j, \dot{\mathbf{x}}_j, \mathbf{q}_a, \Omega) = \mathbf{f}(t, \mathbf{x}, \mathbf{q}_a, \Omega), \tag{7a}$$

$$\dot{\mathbf{x}} = \mathbf{f}(\mathbf{p}, \mathbf{q}, \dot{\mathbf{q}}, \mathbf{x}_j, \dot{\mathbf{x}}_j, \mathbf{q}_a, \Omega) = \mathbf{f}(\mathbf{x}, \mathbf{q}_a, \Omega), \tag{7b}$$

where

$$\mathbf{x} = \left\{ \mathbf{p} \quad \mathbf{q} \quad \dot{\mathbf{q}} \quad \mathbf{x}_j \quad \dot{\mathbf{x}}_j \right\}^{\mathrm{T}} \quad \text{and}$$

$$\dot{\mathbf{x}} = \left\{ \dot{\mathbf{p}} \quad \dot{\mathbf{q}} \quad \ddot{\mathbf{q}} \quad \dot{\mathbf{x}}_j \quad \ddot{\mathbf{x}}_j \right\}^{\mathrm{T}}.$$

In equations (7), $\mathbf{f}$ is the vector field that describes how the state variables of the system evolve over time, as a function of the current state and the external input (elongation of the actuators). Note that the system described in equation (7a) has the time appearing explicitly in the vector field $\mathbf{f}$, therefore it is a non-autonomous system. If the unbalance grade is zero, i.e. the rotor is perfectly balanced, the system described in equation (7b) is autonomous.

In equations (7a) and (7b), $\mathbf{x}_j = \left\{ x_1 \quad x_2 \quad x_3 \quad x_4 \right\}^{\mathrm{T}}$ is the vector containing the lateral displacements and velocities of the center of the disc. The total number of state variables used to describe the response of the system is $N = 491$. Simulation results of the open loop system follow for both bearing geometries, with different unbalance grades (see Figs. 4 and 5).

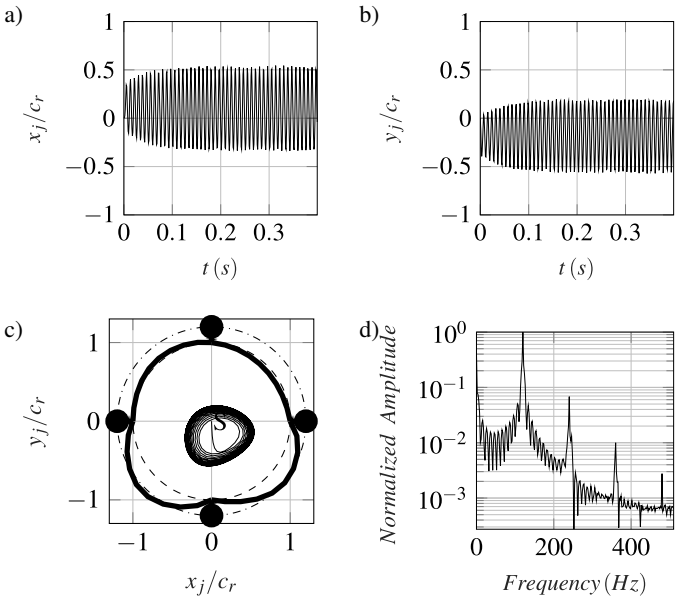

Fig. 4. a) x-displacement, b) y-displacement, c) orbit, and d) x-displacement signal representation in the frequency domain of the centre of the disc at $\Omega = 1550$ rad/s. Bearing D30, disc mass $m_d = 0.1$ kg, foil thickness $h_f = 0.1$ mm, unbalance grade G2.5

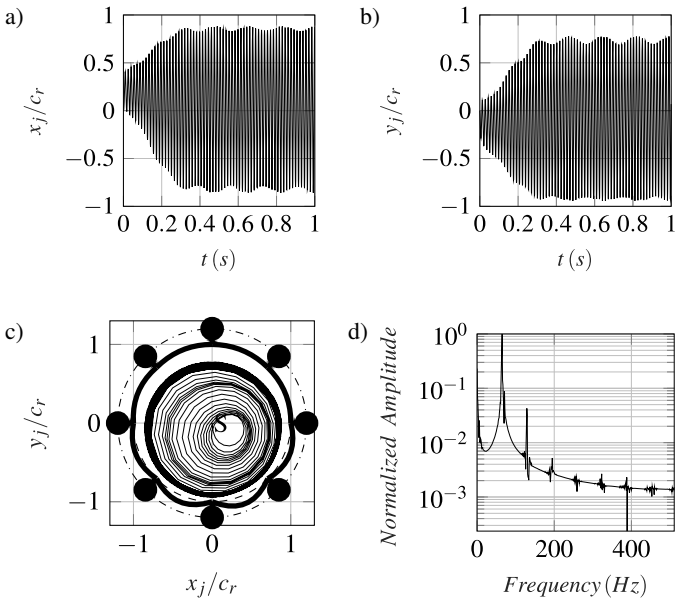

Fig. 5. a) x-displacement, b) y-displacement, c) orbit, and d) x-displacement signal representation in the frequency domain of the centre of the disc at $\Omega = 850$ rad/s. Bearing D100, disc mass $m_d = 1$ kg, foil thickness $h_f = 0.5$ mm, unbalance grade G6.3

3. APPLICATION OF FEEDBACK CONTROL

First, a linear control technique is used, utilizing an observer. Polynomial feedback control laws are also considered, in order to stabilize the equilibrium point and eliminate possible Hopf bifurcations. This technique appears to be applicable in the case of existing unbalance forces and results in steady-state oscillations with decreased amplitude and synchronous period.

3.1. Stabilization via linear control

For fixed elongations of the actuators $\mathbf{q}_a = \mathbf{q}_{a_0}$ and at a specific value of the rotational speed, the system (7b) has a single (unique) equilibrium (fixed) point $\mathbf{x}^*$. The stability of this fixed point is defined by the first Lyapunov criterion, see [26], according to the real parts of the eigenvalues of the Jacobian matrix $\mathbf{A} = \partial\mathbf{f}/\partial\mathbf{x}\Big|_{\substack{\mathbf{x}=\mathbf{x}^*\\ \mathbf{q}_a=\mathbf{q}_{a_0}}}$.

It is supposed that the outputs are the state variables concerning the rotor. The linearized system (equation (8a)) undergoes a coordinate transformation $\delta\mathbf{x}_b = \mathbf{T}_b\delta\mathbf{x}$, into modal coordinates (equation (8b)). Also, a rearrangement of the new state variables is performed in order to separate the stable and unstable subsystems:

$$\delta\dot{\mathbf{x}} = \mathbf{A}\delta bfx + \mathbf{B}\delta\mathbf{q}_a\,, \qquad \delta\mathbf{y} = \mathbf{C}\delta\mathbf{x}, \tag{8a}$$

$$\delta\dot{\mathbf{x}}_b = \mathbf{A}_b\delta\mathbf{x}_b + \mathbf{B}_b\delta\mathbf{q}_a\,, \qquad \delta\mathbf{y} = \mathbf{C}_b\delta\mathbf{x}_b\,, \tag{8b}$$

where $\mathbf{B} = \partial\mathbf{f}/\partial\mathbf{q}_a\Big|_{\substack{\mathbf{x}=\mathbf{x}^*\\ \mathbf{q}_a=\mathbf{q}_{a_0}}}$, $\mathbf{A}_b = \begin{Bmatrix}\mathbf{A}_u & \mathbf{0}\\ \mathbf{0} & \mathbf{A}_s\end{Bmatrix}$, $\mathbf{B}_b = \begin{Bmatrix}\mathbf{B}_u\\ \mathbf{B}_s\end{Bmatrix}$, $\mathbf{C_b} = \begin{Bmatrix}\mathbf{C}_u & \mathbf{C}_s\end{Bmatrix}$.

The unstable (equation (9a)) and stable (equation (9b)) subsystems are defined in equation ((9)):

$$\delta\dot{\mathbf{x}}_u = \mathbf{A}_u\delta\mathbf{x}_u + \mathbf{B}_u\delta\mathbf{q}_a\,, \tag{9a}$$

$$\delta\dot{\mathbf{x}}_s = \mathbf{A}_s\delta\mathbf{x}_s + \mathbf{B}_s\delta\mathbf{q}_a\,. \tag{9b}$$

The closed-loop system is designed only for the unstable subsystem (9a). It was observed that two conjugate eigenvalues cross the imaginary axis and become unstable, therefore the unstable subsystem consists of two state variables. The addition of the observer results in a close loop system of four state variables, the states $\delta\mathbf{x}_u$, and the errors $\delta\tilde{\mathbf{x}}_u$ resulting from the estimation of the observer. The dominant closed-loop eigenvalues are chosen to have the same imaginary part as the eigenvalues of the unstable subsystem, and the real parts are calculated according to the desired setting time $\mathrm{Re}(\lambda_{1,2}) = -4/t_s$. The remaining eigenvalues $\lambda_{3,4}$ are chosen in such a way that the estimations of the observer converge to the actual value of the states ten times faster than the convergence of the states to the equilibrium point. The feedback law is $\delta\mathbf{q}_a = -\mathbf{K}_g\delta\hat{\mathbf{x}}_u$ and the closed-loop system is defined in equation (10), where $\mathbf{K}_g$ and $\mathbf{L}$ are the feedback and the observer gain matrices respectively, and place the eigenvalues $\lambda_{1,2}$, and $\lambda_{3,4}$ at the desired location. They result from the application of Akermann's formula, see [27]. After the solution of the system (10), the system (9b) is solved, and then the state variables $\delta\mathbf{x}$ are calculated:

$$\begin{vmatrix}\delta\dot{\mathbf{x}}_u\\ \delta\dot{\tilde{\mathbf{x}}}_\mathbf{u}\end{vmatrix} = \begin{Bmatrix}\mathbf{A}_u - \mathbf{B}_u\mathbf{K}_g & \mathbf{B}_u\mathbf{K}_g\\ \mathbf{0} & \mathbf{A}_u - \mathbf{L}\mathbf{C}_u\end{Bmatrix}\begin{vmatrix}\delta\mathbf{x}_u\\ \delta\tilde{\mathbf{x}}_u\end{vmatrix}. \tag{10}$$

Figure 6 shows the response of the open and closed-loop system with the bearing D100. Initially (open loop) the equilibrium

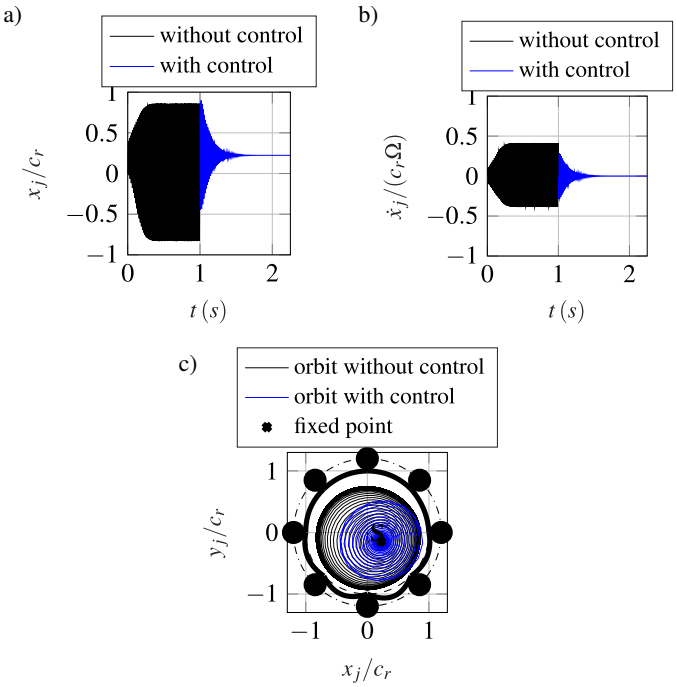

Fig. 6. Open and closed loop a) x-displacement, b) velocity, and c) orbit of the center of the disc at $\Omega = 850$ rad/s. Linear control, bearing D100, disc mass $m_d = 1$ kg, balanced rotor

point is unstable and a self-excited oscillation is observed. The orbit of the centre of the disc is attracted by a stable limit cycle, see Fig. 6c. After the initiation of the control (closed-loop system) the orbit of the centre of the disc is attracted by the stable fixed point, see Fig. 6c and the x-velocity becomes zero after finite time. In this case it was chosen $t_s = 0.5$ s. The behaviour of the system with the bearing D30 is identical, see Fig. 7. In this case, the setting time was chosen to be $t_s = 0.1$ s.

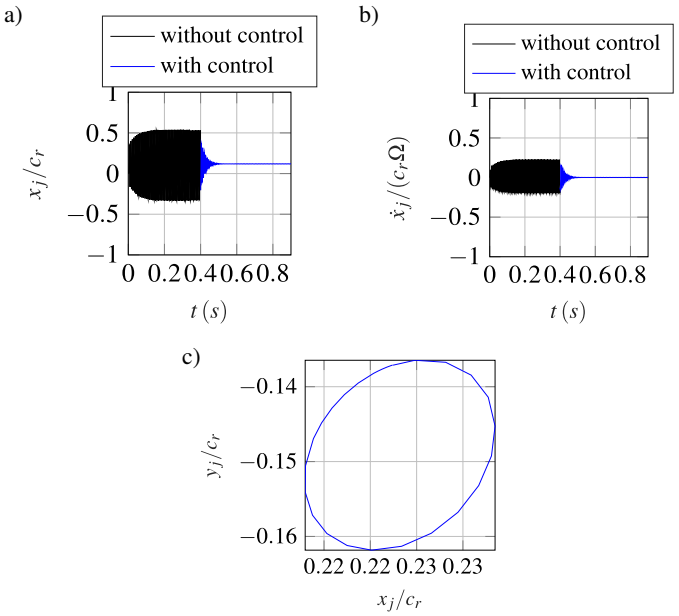

Fig. 7. Open and closed loop a) x-displacement, b) velocity, and c) orbit of the center of the disc at $\Omega = 1550$ rad/s. Linear control, bearing D30, disc mass$m_d = 0.1$ kg, balanced rotor

3.2. Stabilization via polynomial feedback

From equation (1) it is shown that there is a linear dependence of the time derivatives of the states on the elongation of the actuators. Therefore, the state equations of the balanced system can be written in the form of equation (11), where $\mathbf{G}$ is a constant matrix calculated from equation (1). The goal is to stabilize the equilibrium points of equation (12) for every discrete value of the rotational speed and fixed elongation of the actuators, $\mathbf{q}_{a_0}$, namely the fixed point of the system:

$$\dot{\mathbf{x}} = \mathbf{f}(\mathbf{x}, \mathbf{q}_a, \Omega) = \mathbf{g}(\mathbf{x}, \Omega) + \mathbf{G}\,\mathbf{q}_a\,, \tag{11}$$

$$\dot{\mathbf{x}} = \mathbf{f}\left(\mathbf{x}, \mathbf{q}_{a_0}, \Omega_k\right) = \mathbf{f}\left(\mathbf{x}, \mathbf{q}_{a_0}\right) = \mathbf{g}(\mathbf{x}) + \mathbf{G}\,\mathbf{q}_{a_0}\,. \tag{12}$$

A linear polynomial feedback law, proposed by Chen, is defined in equation (13), where$x_j^*, \dot{x}_j^*, y_j^*, \dot{y}_j^*$ are the equilibrium components corresponding to the journal:

$$\begin{aligned}\mathbf{q}_a = &-\mathbf{k}_1\left(x_j - x_j^*\right) - \mathbf{k}_2\left(\dot{x}_j - \dot{x}_j^*\right)\\ &-\mathbf{k}_3\left(y_j - y_j^*\right) - \mathbf{k}_4\left(\dot{y}_j - \dot{y}_j^*\right) + \mathbf{q}_{a_0}\,.\end{aligned} \tag{13}$$

First-order polynomials are adequate for the shifting of Hopf bifurcations to higher rotating speeds. Investigation of the use of second- and higher-order polynomials and the control of the amplitude of the emerging limit cycles is part of ongoing research. The gain vectors $\mathbf{k}_i$ are such that the Jacobian matrix corresponding to the closed-loop system has only eigenvalues with negative real parts. Also, they can be chosen in such a way that the dominant eigenvalues have real parts corresponding to a desired setting time. For simplicity, the gains are chosen in such a way that $\mathbf{k}_i = k_i \begin{vmatrix} 1 & 1 & \cdots & 1 \end{vmatrix}^{\mathrm{T}}$. The gains are calculated using an optimization procedure, calculating the Jacobian matrix at each step. The objective function is defined in equation (14) after choosing the desired t_s:

$$\min\left(\mathrm{obj}\right) = \left|\mathrm{Re}\left(\lambda_{1,2}\right) + 4/t_s\right|. \tag{14}$$

For the implementation of the above, the *patternsearch* function of the *Matlab Global Optimization Toolbox* [28] was used. In Fig. 8 the response of the disc center for the system of bearing D100 is shown. The qualitative behaviour of the open and closed-loop system is similar to that in Fig. 6. The setting time is chosen to be $t_s = 0.5$ s. The actuators in the middle plane are moving, while the actuators in the front and rear plane are static (see Fig. 2b). The same feedback law can be applied in the case of existing unbalance. The steady state response of the system is a limit cycle with suppressed amplitude and synchronous period, as shown in Fig. 9. For the bearing D30, the polynomial feedback law is used to stabilize the fixed points in the entire operational range. The dominant eigenvalues of the open-loop system are shown in Fig. 10a. The gains of the closed-loop system for every value of the rotational speed, as

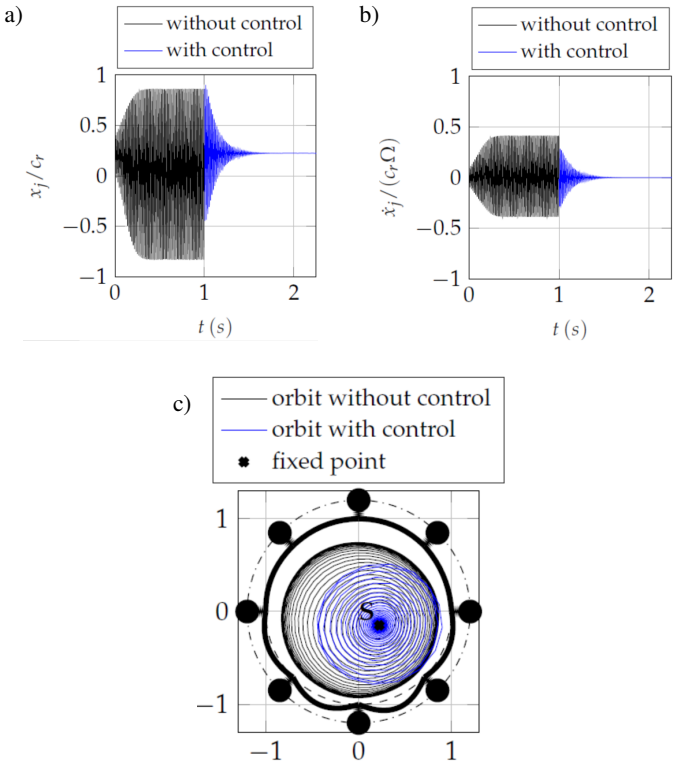

Fig. 8. Open- and closed-loop a) x-displacement, b) velocity, and c) orbit of the center of the disc at $\Omega = 850$ rad/s. Polynomial feedback control, bearing D100, disc mass $m_d = 1$ kg, balanced rotor

shown in Fig. 10b, with initially unstable fixed point are chosen in such a way, that the dominant eigenvalues of the closed-loop system (see Fig. 10c) correspond to setting time $t_s = 0.5$ s.

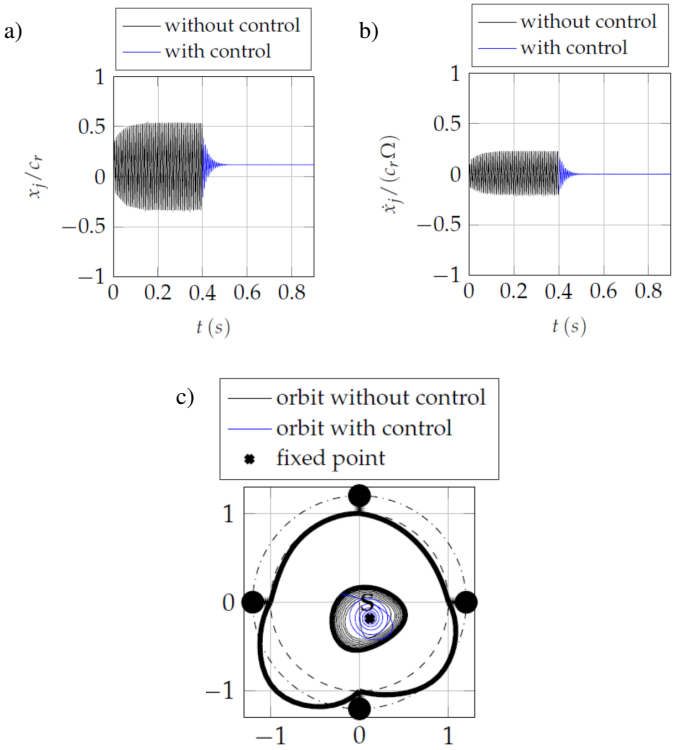

Fig. 9. Open and close loop a) x-displacement, b) velocity, and c) orbit of the center of the disc at $\Omega = 850$ rad/s. Polynomial feedback control, bearing D100, disc mass $m_d = 1$ kg, unbalance grade G6.3

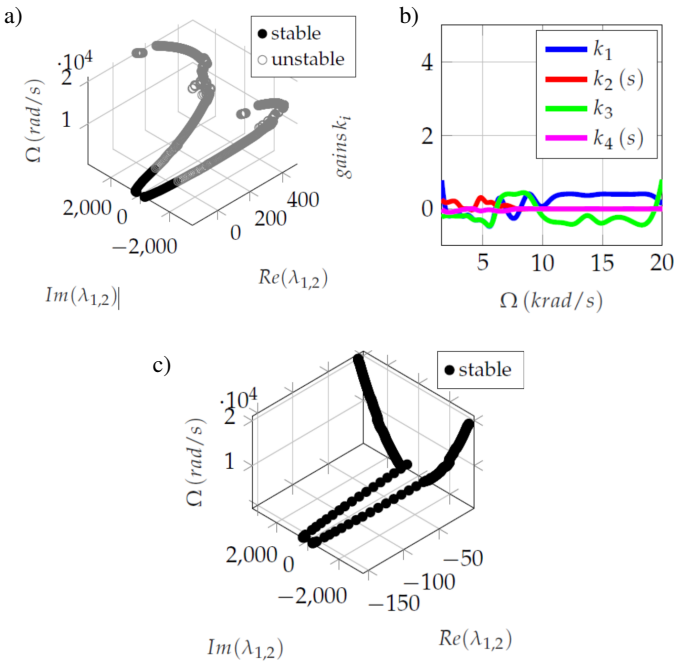

Fig. 10. a) open loop dominant eigenvalues, b) feedback gains for every value of the rotational speed with initially unstable fixed point, and c) close loop dominant eigenvalues

4. CONCLUSIONS

In conclusion, linear polynomial feedback and classic linear control theory are found to be sufficient for the stabilization of fixed-point equilibria in rotor AGFB systems of small and large diameters, and with high or low loading. More specifically:

1. The D30 bearing was stabilized at the speed of $\Omega = 1550$ rad/s and the D30 bearing was stabilized at $\Omega = 850$ rad/s when classic linear feedback control or polynomial feedback control was applied.
2. Stabilization at speeds up to $\Omega = 20$ krad/s (191 kRPM) was found to be feasible, and with relatively low control gains, for the D30 bearing.
3. The proposed AGFB, when stabilized, did not produce oscillation amplitudes which would compromise the integrity and the operability of the element. Gas film thickness was retained in acceptable values.
4. The AGFB was able to attract self-excited limit cycle motions of large (close to radial clearance) or low extent, around stable fixed points, at both D30 and D100 bearings. The system executed stable whirling of small (or minor) amplitude around the stabilized fixed-point equilibrium. This was verified by time integration at several speeds.

For the elimination of Hopf bifurcations and the stabilization of the system around fixed points, the gains must be chosen in a way that a specification, like the setting time, is satisfied. It is found that evaluating the gains through an optimization problem is sufficient to achieve the desired response in terms of stability and time constant.

Future theoretical work to be performed includes nonlinear terms in the feedback function, in order to control the amplitude and the minimal period of self-excited limit cycle motions of the balanced or the unbalanced system.

ACKNOWLEDGEMENTS

The authors would like to acknowledge the Alexander von Humboldt Foundation (Germany), and the Hellenic Foundation for Research and Innovation (Greece) - Fellowship Number 9575, for the funding of this work.

REFERENCES

[1] T. Leister, C. Baum, and W. Seemann, "On the importance of frictional energy dissipation in the prevention of undesirable self-excited vibrations in gas foil bearing rotor systems," *Technische Mechanik*, vol. 37, pp. 280–290, 2017, doi: 10.24352/UB.OVGU-2017-104.

[2] H. Heshmat, J.A. Walowit, and O. Pinkus, "Analysis of Gas-Lubricated Foil Journal Bearings," *J.Lubr. Technol.*, vol. 105, no. 4, pp. 647–655, 1983, doi: 10.1115/1.3254697.

[3] J.S. Larsen, I.F. Santos, and S. von Osmanski, "Stability of rigid rotors supported by air foil bearings: Comparison of two fundamental approaches," *J. Sound Vibr.*, vol. 381, pp. 179–191, 2016, doi: 10.1016/j.jsv.2016.06.022.

[4] S.P. Bhore and A.K. Darpe, "Nonlinear dynamics of flexible rotor supported on the gas foil journal bearings," *J. Sound Vibr.*, vol. 332, no. 20, pp. 5135–5150, 2013, doi: 10.1016/j.jsv.2013.04.023.

[5] D. Kim, "Parametric Studies on Static and Dynamic Performance of Air Foil Bearings with Different Top Foil Geometries and Bump Stiffness Distributions," *J. Tribol.*, vol. 129, no. 2, pp. 354–364, 2006, doi: 10.1115/1.2540065.

[6] J.S. Larsen and I.F. Santos, "On the nonlinear steady-state response of rigid rotors supported by air foil bearings – theory and experiments," *J. Sound Vibr.*, vol. 346, pp. 284–297, 2015, doi: 10.1016/j.jsv.2015.02.017.

[7] J.W. Lund, "Calculation of Stiffness and Damping Properties of Gas Bearings," *J. Lubr. Technol.*, vol. 90, no. 4, pp. 793–803, 1968, doi: 10.1115/1.3601723.

[8] B.B. Nielsen and I.F. Santos, "Transient and steady state behaviour of elasto–aerodynamic air foil bearings, considering bump foil compliance and top foil inertia and flexibility: A numerical investigation," *Proc. Inst. Mech. Eng. Part J.-J. Eng. Tribol.*, vol. 231, no. 10, pp. 1235–1253, 2017, doi: 10.1177/1350650117689985.

[9] H. Pham and P. Bonello, "Efficient techniques for the computation of the nonlinear dynamics of a foil-air bearing rotor system," in *Proc. ASME Turbo Expo 2013: Turbine Technical Conference and Exposition. Volume 7B: Structures and Dynamics*, USA, 2013, p. V07BT30A011, doi: 10.1115/GT2013-94389.

[10] P. Bonello and H.M. Pham, "Nonlinear Dynamic Analysis of High Speed Oil-Free Turbomachinery With Focus on Stability and Self-Excited Vibration," *J. Tribol.*, vol. 136, no. 4, p. 041705, 2014, doi: 10.1115/1.4027859.

[11] T. Pronobis and R. Liebich, "Comparison of stability limits obtained by time integration and perturbation approach for gas foil bearings," *J. Sound Vibr.*, vol. 458, pp. 497–509, 2019, doi: 10.1016/j.jsv.2019.06.034.

[12] J. Park and K. Sim, "A Feasibility Study of Controllable Gas Foil Bearings With Piezoelectric Materials Via Rotordynamic Model Predictions," *J. Eng. Gas. Turbines Power-Trans. ASME*, vol. 141, no. 2, p. 021027, 2018, doi: 10.1115/1.4041384.

[13] L. Savin, D. Shutin, and A. Kuzavka, "Actuators of active tribotechnical systems of the rotor-bearing type," in *IOP Conference Series: Materials Science and Engineering*, vol. 233, no. 1, p. 012043, 2017, doi: 10.1088/1757-899X/233/1/012043.

[14] A. Chasalevris and F. Dohnal, "A journal bearing with variable geometry for the reduction of the maximum amplitude during passage through resonance," *J. Vib. Acoust.*, vol. 134, no. 6, p. 061005, 2012, doi: 10.1115/1.4007242.

[15] A. Chasalevris and F. Dohnal, "A journal bearing with variable geometry for the suppression of vibrations in rotating shafts: Simulation, design, construction and experiment," *Mech. Syst. Signal Proc.*, vol. 52–53, no. 1, pp. 506–528, 2015, doi: 10.1016/j.ymssp.2014.07.002.

[16] A. Chasalevris and G. Guignier, "Alignment and rotordynamic optimization of turbine shaft trains using adjustable bearings in real-time operation," *Proc. Inst. Mech. Eng. Part C-J. Eng. Mech. Eng. Sci.*, vol. 233, no. 7, pp. 2379–2399, 2019, doi: 10.1177/0954406218791636.

[17] S. von Osmanski and I.F. Santos, "Gas foil bearings with radial injection: Multi-domain stability analysis and unbalance response," *J. Sound Vibr.*, vol. 508, p. 116177, 2021, doi: 10.1016/j.jsv.2021.116177.

[18] S.-H. Chen and H.H. Pan, "Guyan reduction," *Commun. Appl. Num. Meth.*, vol. 4, no. 4, pp. 549–556, 1988, doi: 10.1002/cnm.1630040412.

[19] P. Yu and G. Chen, "Hopf bifurcation control using nonlinear feedback with polynomial functions," *Int. J. Bifurcation Chaos*, vol. 14, no. 05, pp. 1683–1704, 2004, doi: 10.1142/S0218127404010291.

[20] M. Bonnet, A. Frangi, and C. Rey, *The finite element method in solid mechanics*. McGraw Hill Education, 2014. [Online]. Available: https://hal.science/hal-01083772.

[21] E. Estupinan and I. Santos, "Controllable Lubrication for Main Engine Bearings Using Mechanical and Piezoelectric Actuators," *IEEE/ASME Trans. Mechatron.*, vol. 17, no. 2, pp. 279–287, 2012, doi: 10.1109/TMECH.2010.2099663.

[22] E.A. Estupinan and I.F. Santos, "Controllable radial oil injection applied to main engine bearings-hybrid bearing configurations and control pressure rules," *Proc. STLE/ASME 2010 International Joint Tribology Conference. STLE/ASME 2010 International Joint Tribology Conference*, USA, 2010, pp. 145–147, doi: 10.1115/IJTC2010-41170.

[23] ANSI/IEEE, 1987. IEEE standard on piezoelectricity. Tech. Rep. Std 176-1987, IEEE Ultrasonics, Ferroelectrics, and Frequency Control Society, New York.

[24] A. Duvnjak and E. Marusic-Paloka, "Derivation of the reynolds equation for lubrication of a rotating shaft," *Arch. Math.*, vol. 036, no. 4, pp. 239253, 2000. [Online]. Available: http://eudml.org/doc/248566.

[25] P. Papafragkos, I. Gavalas, I. Raptopoulos, and A. Chasalevris, "Optimizing energy dissipation in gas foil bearings to eliminate bifurcations of limit cycles in unbalanced rotor systems," *Nonlinear Dyn.*, vol. 111, no. 1, pp. 67–95, 2023, doi: 10.1007/s11071-022-07837-1.

[26] C. Pukdeboon, "A review of fundamentals of Lyapunov theory," *J. Appl Sci.*, vol. 10, no. 01, pp. 55–61, 2011.

[27] J. van der Woude, "A note on pole placement by static output feedback for single-input systems," *Syst. Control Lett.*, vol. 11, no. 4, pp. 285–287, 1988, doi: 10.1016/0167-6911(88)90072-2.

[28] The MathWorks, Inc. (2022). *Optimization Toolbox version: R2021b*. [Online] Available: https://www.mathworks.com.